Numerical modeling of the coupled seismoelectric wave propagation in frequency domain

Mehran Gharibi, R. Arief Budiman, Robert R. Stewart, and Laurence R. Bentley

ABSTRACT

Theoretical developments in the last decade suggest that seismoelectric responses are sensitive to the fluid content of the subsurface structures. The objectives of this study are to i) conduct theoretical and experimental studies to examine the properties of the coupled seismic and electromagnetic field disturbances in saturated porous media and ii) assess the potential of the seismoelectric and seismomagnetic techniques in detecting and evaluating deep structures such as hydrocarbon reservoirs. We describe our numerical modeling, in the frequency domain, of the generation of electromagnetic waves induced by seismic waves launched by surface explosions using FEMLAB. We have completed the frequency-domain simulations on a homogeneously porous semi-infinite solid. The three-dimensional simulations were based on three coupled partial differential equations involving the electric field, the solid-phase elastic displacement, and the relative displacement between the solid and the fluid phase. While the lateral components of the relative displacement do not appear to have any particular pattern, the resulting z-component of the electric field shows a macroscopic vertical dipole response. The solid-phase displacement agrees with the analytical results.

INTRODUCTION

The propagation of coupled electromagnetic and seismic waves in saturated porous media has been discussed by several authors (e.g. Pride, 1994; Pride and Haartsen, 1996; Garambois and Dietrichz, 2001; Thompson and Gist, 1993). The coupling is described by electrokinetic phenomena which occur at the solid-fluid interface. The electric double-layer formed at the surface of the solid grain, which is balanced by diffusive counter ions extending into the liquid phase, gives rise to an electrical potential at a microscopic scale. Relative charge displacements in the pore space caused by the propagation of an elastic wave through such a medium generate electrokinetic coupling or seismoelectric phenomena.

To model the propagation of a coupled electric and mechanical disturbance in a semi-infinite homogenous porous medium, we follow the derivation of the seismoelectric model by Pride (1994). There are nine coupled differential equations describing the interaction between acoustic and electromagnetic waves.

$$\nabla \times \boldsymbol{E} = -i\omega\boldsymbol{B}, \tag{1}$$

$$\nabla \times \boldsymbol{H} = i\omega\boldsymbol{D} + \boldsymbol{J}, \tag{2}$$

$$\nabla \cdot \tau_B = -\omega^2 (\rho_B \boldsymbol{u_s} + \rho_f \boldsymbol{w}), \tag{3}$$

$$\boldsymbol{J} = \sigma(\omega)\boldsymbol{E} + \boldsymbol{L}(\omega)(-\nabla p + \omega^2 \rho_f \boldsymbol{u_s}), \tag{4}$$

$$-i\omega\boldsymbol{w} = \boldsymbol{L}(\omega)\boldsymbol{E} + \frac{k(\omega)}{\eta}\left(-\nabla p + \omega^2 \rho_f \boldsymbol{u_s}\right), \tag{5}$$

$$\boldsymbol{D} = \varepsilon_0 \left[\frac{\Phi}{\alpha_\infty}(\kappa_f - \kappa_s) + \kappa_s \right]\boldsymbol{E}, \tag{6}$$

$$\boldsymbol{B} = \mu_0 \boldsymbol{H}, \tag{7}$$

$$\tau_B = \left(K_G \nabla \cdot \boldsymbol{u}_s + C\nabla \cdot \boldsymbol{w}\right)\boldsymbol{I} + G_{fr}(\nabla \boldsymbol{u}_s + \nabla \boldsymbol{u_s^T} - \frac{2}{3}\nabla \cdot \boldsymbol{u}_s \boldsymbol{I}), \tag{8}$$

$$-p = C\nabla \cdot \boldsymbol{u}_s + M\nabla \cdot \boldsymbol{w}, \tag{9}$$

where ω is the angular frequency, H is the magnetic field, B is magnetic flux density, E is the electric field, D is the electric displacement field, J is the current density, ε_0 is the dielectric permittivity of free air, ϕ is the porosity, α_∞ is the tortuosity, κ_s is the dielectric constant of the solid, κ_f is the dielectric constant of the liquid, μ_0 is the magnetic permeability, L is the coupling coefficient, K_G, C, M, and G_{fr} are elastic constants of the porous medium, ρ_f is the fluid density, ρ_s is the solid density, ρ_B is the bulk density, k is a transport coefficient, η is the viscosity, u_s is the solid displacement, p is the fluid pressure, τ_B is the bulk stress tensor, and w is the relative solid-liquid displacement.

These equations describe three three-dimensional vector fields: the solid-phase displacement, the relative displacement between the solid and the liquid phases, and the electric field generated. Auxiliary vector fields, including magnetic and electric polarizations, can be derived from the fundamental three vector fields. In addition, fluid pressure can be obtained from the divergences of the solid-phase and the solid-liquid displacement fields.

THEORETICAL DEVELOPMENT AND NUMERICAL MODELING

We use the FEMLAB software package as our standard modeling software. FEMLAB is an interactive partial differential equation (PDE) solver used for simulating physical processes that can be described as PDEs. In the following, we briefly review the manipulation of the governing equations (1) to (9) that we have adopted for computer implementation, and the numerical modeling.

The nine governing equations are Fourier-transformed to produce frequency-dependent equations. They can be further reduced into three coupled equations below:

$$\nabla \times \nabla \times \boldsymbol{D} = \omega^2 \varepsilon_0 \left[\frac{\Phi}{\alpha_\infty}(\kappa_f - \kappa_s) + \kappa_s \right] \mu_0 \boldsymbol{D} + i\omega \mu_0 \sigma \boldsymbol{D} +$$

$$i\omega \varepsilon_0 \mu_0 L \left[\frac{\Phi}{\alpha_\infty}(\kappa_f - \kappa_s) + \kappa_s \right] \times \left(\nabla \{ C\nabla \cdot \boldsymbol{u}_s + M\nabla \cdot \boldsymbol{w} \} + \omega^2 \rho_f \boldsymbol{u}_s \right), \tag{10}$$

and

$$-i\omega \boldsymbol{W} = \frac{L\boldsymbol{D}}{\varepsilon_0 \left[\dfrac{\Phi}{\alpha_\infty}(\kappa_f - \kappa_s) + \kappa_s \right]} + \frac{k}{\eta} \left(C\nabla(\nabla \cdot \boldsymbol{u}_s) + M\nabla(\nabla \cdot \boldsymbol{w}) + \omega^2 \rho_f \boldsymbol{u}_s \right), \tag{11}$$

and

$$-\omega^2 (\rho_B \boldsymbol{u}_s + \rho_f \boldsymbol{w}) = K_G \nabla \cdot (\nabla \cdot \boldsymbol{u}_s \boldsymbol{I}) + C\nabla \cdot (\nabla \cdot \boldsymbol{w} \boldsymbol{I}) +$$

$$G_{fr} \nabla \cdot (\nabla \boldsymbol{u}_s + \nabla \boldsymbol{u}_s^T - \frac{2}{3} \nabla \cdot \boldsymbol{u}_s \boldsymbol{I}) \tag{12}$$

Equations (10), (11) and, (12) were implemented in FEMLAB using two structural mechanics modules and one PDE module to solve for the solid phase, solid-liquid phase, and the electric fields.

RESULTS AND DISCUSSION

The FEMLAB software package has several built-in modules for different applications with the option to add more modules. The software also allows entering the equations as a set of PDEs. A series of models were created to examine the various methods of implementing the equations into FEMLAB.

A homogenous, half-space earth model was used in the modeling. The differences between various models were the size and geometry of the grids as well as boundary conditions. The main objectives at this point were to i) verify the accuracy of the FEMLAB results, ii) explore the best ways to implement the equations, and iii) the optimum parameters for modeling. So far, the modeling has been conducted in the frequency domain by solving the governing equations for each frequency. In principle, the time-dependent solutions can be obtained using an inverse Fourier transform over a large frequency band, however, this is not practical since there are about 100,000 nodes and for each node there are 9 vector field components. We are planning to add a time-dependent electromagnetic module to the software package with which modeling in the

time domain will be possible. This decision was reached since most geophysicists and geologists use time-dependent spatial information. We also believe the time-dependent modeling can enhance the presentation of our results.

We conducted a few tests for modeling the acoustic wave generation using the built-in structural mechanics module as well as the PDE mode and compared the results with the analytic solution. We found out that the PDE mode usually does not produce accurate results. Since we will need to implement our complete coupled seismoelectric equations using the PDE mode we are working with the software provider trying to resolve this problem. We determined that using the structural mechanics module made by FEMLAB was more accurate than using the PDEs governing the effect in the PDE mode, despite the fact that they are governed by an identical set of equations.

In the following, we review the preliminary results of the numerical modeling with one of the cube models of size 1000m × 1000m × 500m. It represents closely the results from the other models with smaller size and different grid geometry. The excitation to the semi-infinite soil is provided by a concentrated push force (a very sharp Gaussian profile) on the surface, centered at the top face of the cube, with a magnitude of 1 MN. The boundary condition on the surface for the solid-liquid relative displacement and the electric field are of Neumann type. The Neumann boundary conditions allow for a generation of such fields on the surface since physically the surface may be saturated with the liquid phase as well.

While the surface boundary conditions (at $z = 0$) are of Neumann type, the boundary conditions at the side faces and the bottom face of the cube are zero (Dirichlet type). We performed many numerical tests to ensure that these Dirichlet conditions are reasonable. We find the lateral size (along the x and y axes) is large enough; however, a depth of 500 m may not be sufficient since the decay tails of the fields seem to be truncated too early to become zero.

Each simulation runs for 48 hours for a frequency scan of 0-100 Hz with a 10 Hz increment. Each simulation uses up to 2.5 Gb of RAM on a dual-processor G5 Mac computer. There are typically 300,000 degrees of freedom as each node supports three vector fields, each having three components. The number of nodes in each simulation, therefore, numbers typically 33,000. This massive simulation effort puts a huge restriction on our capacity to run parallel simulations. We hope to solve this limitation in the next 6 months of the project.

Figure 1 shows the typical combined arrow and slice plots of the simulation results in the frequency domain. It shows slice plots for the z-component of the electric field at different depths as well as arrow plots of the z-component of the solid elastic displacement at 100 Hz. The electric field generated by the elastic excitation on the surface has a patterned electric signature. We cannot determine whether the pattern is that of a dipole or a quadrupole; further study is needed.
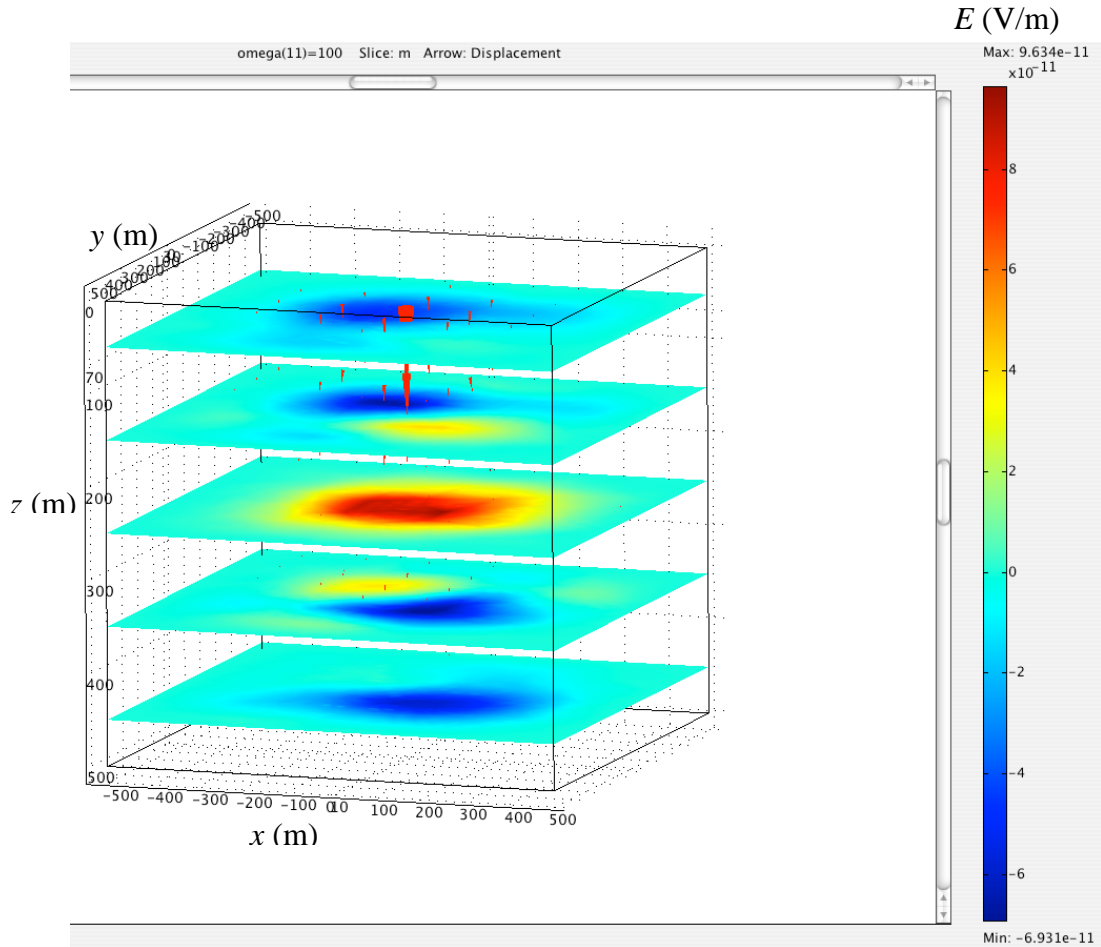
FIG. 1. Slice plots in the frequency domain at different depths for the z-component of the electric field at 100 Hz. The arrows show the z-component of the solid elastic displacement. The plot clearly shows a lateral electric dipole field that alternates in polarity with depth.

   Figure 2 shows the typical z-component of the solid-liquid relative displacement in frequency domain. The pattern shown is much less regular than that of the electric field in Fig. 1. We have checked that the relative-displacement pattern is not related to round-off errors or mesh-size effects according to FEMLAB technical support staff. The pattern decays monotonically with depth. We also determined that the pattern is not due to the symmetry of the cube, i.e., it is not dependent on the cube edges.
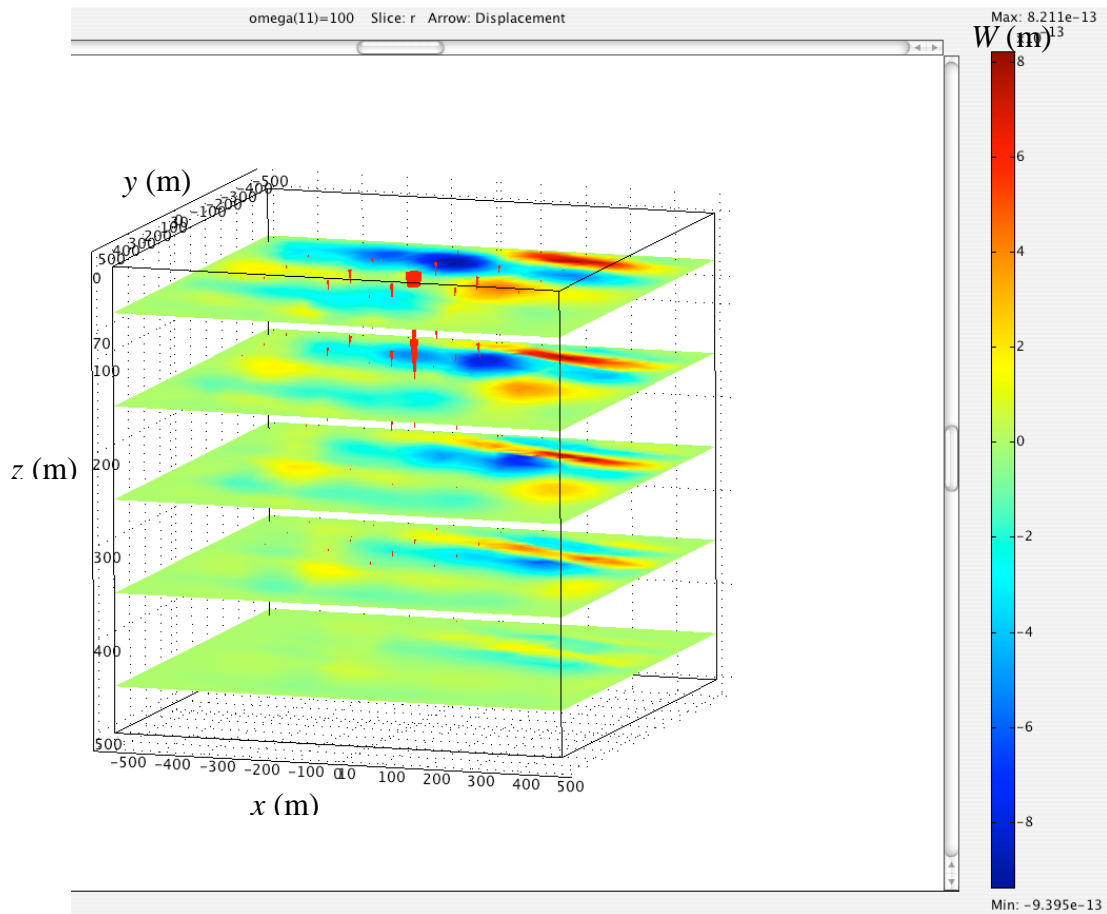
FIG. 2. Slice plots in the frequency domain at different depths for the z-component of the solid-liquid relative displacement at 100 Hz. The arrows show the z-component of the solid elastic displacement.

The accepted understanding of the electromagnetic wave generation from the elastic excitation is that the generation is caused by the relative motion of the fluid phase with respect to the solid phase. Before running the simulations, we were expecting that the solid-liquid displacement pattern determines the electric field pattern. More precisely, the energy flows from the elastic excitation to the solid-liquid elastic displacement before the electromagnetic waves are generated. Figures 1 and 2 do not show this expected behavior.
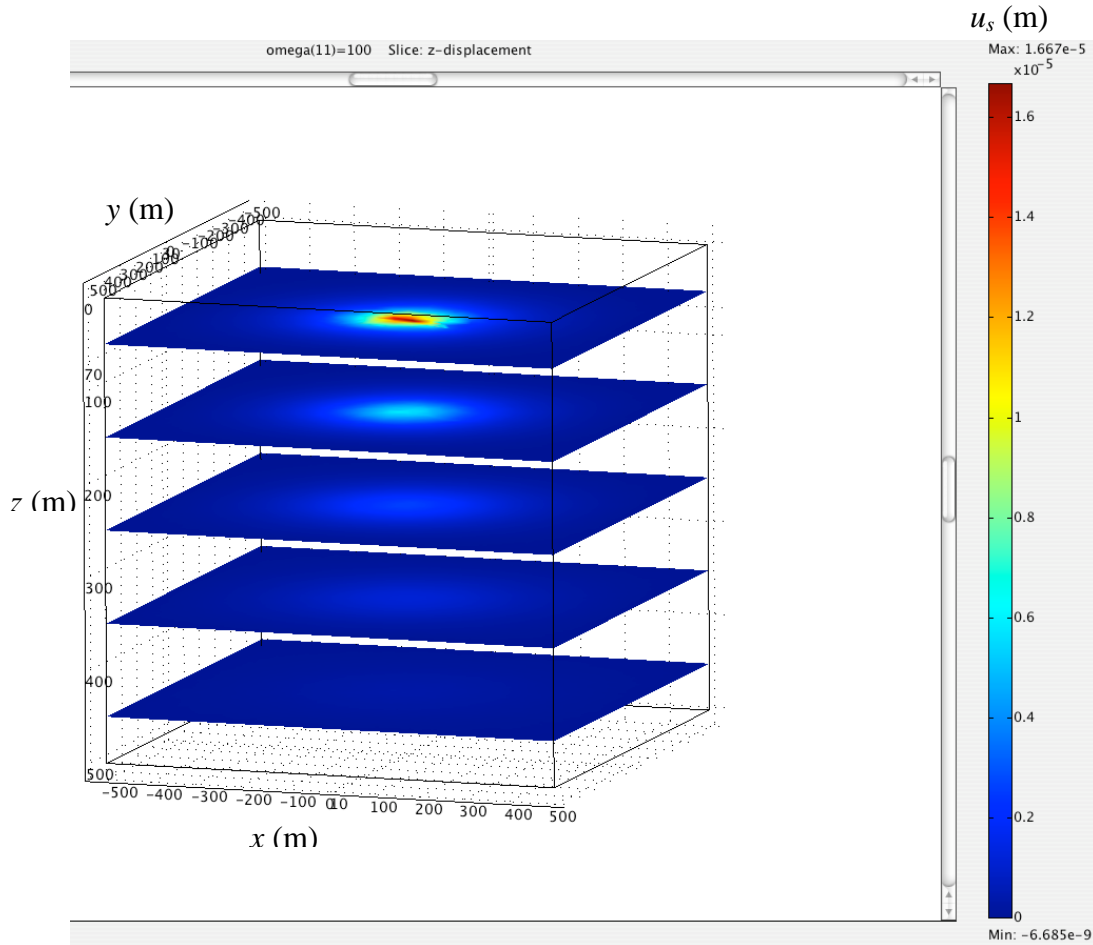
FIG. 3. Slice plots in the frequency domain at different depths for the z-component of the elastic displacement at 100 Hz.

Figure 3 shows the typical z-component of the elastic displacement in frequency domain. Along the depth direction, the displacement decays as 1/z as expected. The lateral pattern is almost circular around the impact point where the push force is applied. The pattern shown by the solid-liquid relative displacement thus seems to be intrinsic within the governing equations, for a lack of physical explanation. A nonlinear effect related to the fluid motion is a possible cause for the pattern generation. It should be easier for the fluid phase to spread the energy since the fluid motion is less attenuated than the solid motion. One numerical test we plan to do is to turn off the liquid viscosity term; in this case, we expect a more enhanced lateral spreading of the relative displacement field.

REFERENCES

Garambois, S. and Dietrichz, M., 2001, Seismoelectric wave conversions in porous media: Field measurements and transfer function analysis: Geophysics, **66**, 1417-1430.

Pride S.R., 1994, Governing equations for the coupled electromagnetics and acoustics of porous media: Phys. Rev. B., **50**, 15678-15696.

Pride S.R., and Haartsen M.W., 1996, Electroseismic wave properties: J. Acoust. Soc. Am., **100**, 1301-1315.

Thompson, A.H., and Gist, G.A., 1993, Geophysical applications of electrokinetic conversion: The Leading Edge, **12**, 1169-1173.